https://doi.org/10.1007/s41230-018-7211-6

Microstructure and wear characteristics of ATZ ceramic particle reinforced gray iron matrix surface composites

Xue Ma [1], *Liang-feng Li [1], Fan Zhang [1,2], Zu-hua Zhang [3], Hao Wang [3], and En-ze Wang [1]

1. School of Materials Science and Engineering, Southwest University of Science and Technology, Mianyang 621010, China

2. Chengdu Aerospace Superalloy Technology Co.,Ltd, Chengdu 610207, China

3. Centre for Future Materials, University of Southern Queensland, Toowoomba, QLD, 4350, Australia

Abstract: The alumina toughened zirconia (ATZ) ceramic particle reinforced gray iron matrix surface composite was successfully manufactured by pressureless infiltration. The porous preform played a key role in the infiltrating progress. The microstructure was observed by scanning electron microscopy (SEM); the phase constitutions was analyzed by X-ray diffraction (XRD); and the hardness and wear resistance of selected specimens were tested by hardness testing machine and abrasion testing machine, respectively. The addition of high carbon ferrochromium powders leads to the formation of white iron during solidification. The wear volume loss rates of ATZ ceramic particle reinforced gray iron matrix surface composite decreases first, and then tends to be stable. The wear resistance of the composite is 2.7 times higher than that of gray iron matrix. The reason is a combination of the surface hardness increase of gray iron matrix and ATZ ceramic particles and alloy carbides protecting effect on gray iron matrix.

Key words: metal-matrix surface composites; pressureless infiltrating; particle-reinforcement; surface alloying; wear testing

CLC numbers: TG143.2 **Document code:** A **Article ID:** 1672-6421(2018)03-167-06

Gray iron is one of the most common cast iron and widely used as a kind of cast material due to its low cost, outstanding castability and excellent machinability [1, 2]. However, the poor wear resistance is a fatal weakness for the gray iron. As we all know, wear is one of the main failure modes of metallic materials and about seventy percent of mechanical damage is caused by various forms of wear and tear. The grinding loss not only consumes a lot of metal material, but also causes huge economic loss and heavy casualties. So revealing the mechanism and improving the wear resistance of the gray iron matrix are significant.

The ceramic particle reinforced metal matrix composites (CPRMMCs) can combine the advantages of ceramics and metals, and exhibit relative high strength and wear resistance, so they have attracted more and more attention [3–6]. Ceramic particles, such as wolfram carbide (WC), alumina (Al_2O_3), titanium carbide (TiC) and silicon carbide (SiC), are now commonly used as the particle reinforcement [7–12]. WC ceramic particle reinforced iron matrix surface composites were produced using the V-EPC infiltration casting process by Li et al., and the composites' wear resistance was 1.5–5.2 times higher than that of the high chromium cast iron [13]. WC ceramic particle with good wettability and high hardness was used in the research [10], but its higher price and the greater difference of thermal expansion coefficient from that of iron limit its use in the large scale production. Alumina toughened zirconia (ATZ) ceramic is becoming an important reinforcement particle to iron and steel because of its great performance/price ratio, high hardness, high fracture toughness, and comparable thermal expansion coefficient [14]. ZrO_2-Al_2O_3 ceramic particle reinforced Cr25 matrix composites were fabricated using the infiltration casting process by Zheng et al. [14], and the wear resistance of the composites was 6 times higher than that of the high chromium cast iron matrix.

In addition to the particle reinforcement technique, a surface alloying technique is also widely used to improve the wear resistance of cast iron [15–17].

***Liang-feng Li**

Male, born in 1982, Ph.D., Associate Professor. The focus of his present research is on the metal matrix ceramic composites.

E-mail: liliangfeng@swust.edu.cn

Received: 2017-10-12; Accepted: 2017-11-24

Chromium surface alloyed austempered ductile iron (ADI) was prepared using Tungsten Inert Gas process by Amirsadeghi et al. [18], which presented different surface hardness due to the variation of chromium content. The surface hardness value of the ADI ranged from 895 to 1,080 HV, and the wear rate of the composites reduced from 66% to 38%, respectively [18]. The impact of laser surface alloyed with chromium on the wear performance of gray iron was investigated by Tomlinson et al. [2], and the wear resistance of laser alloyed 17% chromium coating increased 5 times than that of 16% chromium white cast iron.

According to the studies mentioned above, the wear resistances of ceramic particle reinforced metal matrix composites and chromium surface alloyed composites are both better than that of metal matrix, but the wear mechanisms are absolutely different. For ceramic particle reinforced metal matrix composites, the ceramic particles bear the main pressure exerted by the friction test and protect the metal matrix from wear [19]. For chromium surface alloyed composites, the increased surface hardness of the composite with the addition of chromium improves the wear resistance [20]. Combining with the advantages of ceramic particle reinforcement technique and chromium surface alloying technology, the ATZ ceramic particles reinforced gray iron matrix surface composite was manufactured in this work. The phase constitution, microstructure and wear mechanism of the composite were investigated. This work will be of great significance for the application of wear-resistant composites in machinery and manufacturing industries.

1 Experimental procedures

1.1 Preparation of porous preform

3Y-TZP (purity>99.5%, d_{50}=0.36 μm, Jiangxi Farmeiya Materials Co., Ltd., China) and Al_2O_3 powder (purity>99.5%, d_{50}=2.12 μm, Nuoda Chemical Co., Ltd., China) were used as starting materials. ATZ ceramic powder with a 20/80 volume ratio of Al_2O_3/ZrO_2 was first blended by ball milling for 2 h at 100 rpm in an ethanol medium and then uniaxially pressed into a cylindrical pellet under 200 MPa for 30 s in a Φ12 mm stainless mold. The green bodies were sintered at 600 °C for 0.5 h. After crushing and screening, ATZ ceramic particles with sizes ranging from 2 to 4 mm were prepared by sintering at 1,500 °C for 2 h with a heating rate of 2 °C·min^{-1}. The physical and mechanical properties of the ATZ ceramic particles are listed in Table 1.

The porous perform was formed by mixing 55wt.% high carbon ferrochromium powders (HCFPs), 25wt.% ATZ ceramic particles, 2.5wt.% borax, 13wt.% paraffin wax with a diameter of 2–3 mm, and 4.5wt.% water glass. The chemical composition of high carbon ferrochromium powder is shown in Table 2. The homogeneous mixture was poured in a stainless mould with a diameter of 25 mm, and then followed by two-step heating: being heated to 50 °C for 20 min and 100 °C for 2 h. Figure 1 shows the physical photographs of the porous perform with millimeter holes.

Table 1: Physical and mechanical properties of ATZ ceramic particle

Diameter (mm)	Bulk density (g•cm^{-3})	Fracture toughness (MPa•m$^{1/2}$)	Flexural strength (MPa)	Vickers Hardness (GPa)
2–4	5.55–5.61	5.9–6.2	600–670	12.5–12.8

Table 2: Chemical composition of high-carbon ferrochrome powder (wt.%)

C	Si	Cr	P	S	Fe
7.86	1.23	60.27	0.03	0.03	Balance

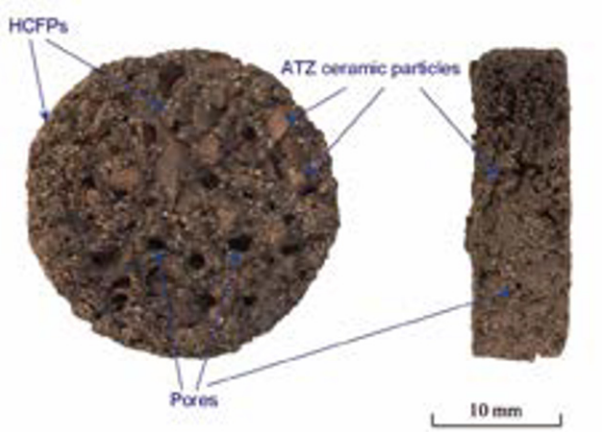

Fig. 1: Physical photograph of porous perform

1.2 Preparation of composite

The porous preforms were placed in the center of the mould cavity, then filled with molten gray iron with a nominal composition of Fe-3.19C-1.21Si-0.39Mn-0.07P-0.07S at 1,370–1,420 °C. The ATZ ceramic particle reinforced and chromium surface alloyed gray iron matrix composite was shaken out of the mold after the casting cooled to the room temperature in air cooling condition.

1.3 Composite characterization and testing

The micro-morphology was observed by 4XC-PC (Shanghai optical instrument factory) optical microscope. Etching was performed using a 4% nital solution. The phase constitutions of the composite was characterized by X-ray diffraction (XRD) on an X′Pert PRO X-ray diffractometer using Cu Kα radiation (λ = 0.154 nm). The XRD spectra were obtained in a range of 10°–100 ° at a scanning rate of 2.5 °·min^{-1}. The microstructure and elemental composition of selected specimens were analyzed by scanning electron microscopy (SEM, Ultra 55, Carl Zeiss) and X-ray energy dispersive spectrometry (EDS, Oxford IE450X-Max80), at a accelerating voltage of 15 kV. The hardness value of the composite was measured using a Vickers hardness testing machine (HBRVU-187.5) under a load of 30 kgf and dwelling time of 15 s. Ten data measurements at different points were collected for the specimen and averaged with the exclusion of

the highest and the lowest hardness points. The microhardness of the metallurgical structure was measured by a HV-1000Z hardness tester under a load of 1 kgf and dwelling time of 15 s.

The friction and wear data were determined according to ASTM G105-02 using an abrasion testing machine (MLS-225, Zhangjiakou Kehua Test Machine Mfg Co., Ltd.). The rubber wheel with a diameter of 178 mm revolved at a rate of 180 rpm under a load of 40 N. The particle sizes of quartz sand abrasive ranged from 0.4 to 0.6 mm in diameter. To ensure the moisture content reached no more than 0.5wt.%, the abrasive particles were dried by heating at 100 °C for 1 h. The friction and wear average data was obtained under the same wear testing conditions at room temperature for 3 times. After wear testing, the worn surfaces of the selected samples were observed again by SEM.

2 Results and discussion

2.1 Optical microscopic morphology observation

Figure 2 shows the optical micrograph of the gray iron matrix composite with ATZ ceramic particle reinforced and chromium surface alloyed. Figure 2(a) is the physical picture of the composite. It can be seen that ATZ ceramic particles uniformly distribute in the surface of the gray iron matrix. The distribution of the ATZ ceramic particles keeps in step with the shape of a porous preform, which indicates that the strength of the porous preform is enough to bear the impact of high-temperature and high flow speed of liquid metal in the casting process. It is also observed that the addition of high carbon ferrochromium powder can lead to the formation of white iron during solidification in the surface of gray iron matrix during solidification [Fig. 2(b)].

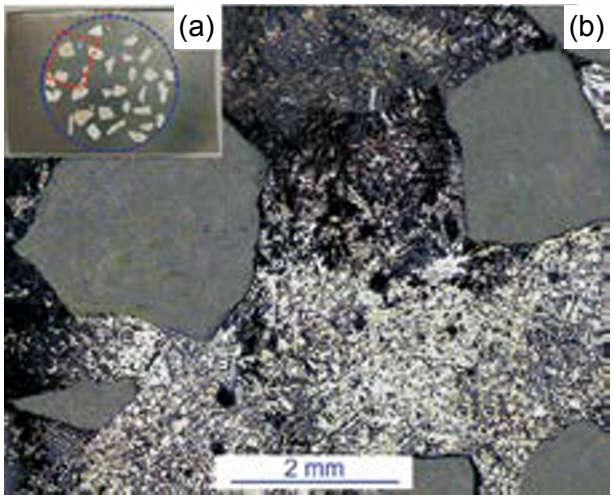

Fig. 2: Physical picture of composite (a) in upper left of corner of optical micrograph of composite (b)

2.2 Phase constitution characterization

Figure 3 presents the XRD patterns of the ATZ ceramic particle reinforced gray iron matrix surface composite. The phase constitutions of the composite consist of ATZ ceramic, α-Fe, γ-Fe, graphite, Fe_7C_3, Cr_7C_3, and Fe_3C. Due to high carbon ferrochromium powder adding into the porous perform, Cr_7C_3 phase and Fe_7C_3 phase can be observed in the surface of the composite. This indicates that chromium alloyed product can be simultaneously obtained in the pressureless infiltration process. It is important to note that the arrangement of Fe atoms in Fe_7C_3 carbides is similar with that of Cr atoms in Cr_7C_3 carbides. Moreover, the atomic radius of Fe (126 pm) is close to that of Cr (128 pm). They can easily replace each other during solidification and do not change the molecular structure of carbides. So these carbides are designated as multi-component compounds $(Fe, Cr)_7C_3$ and $(Fe, Cr)_3C$, which abbreviated are M_7C_3 and M_3C [21, 22].

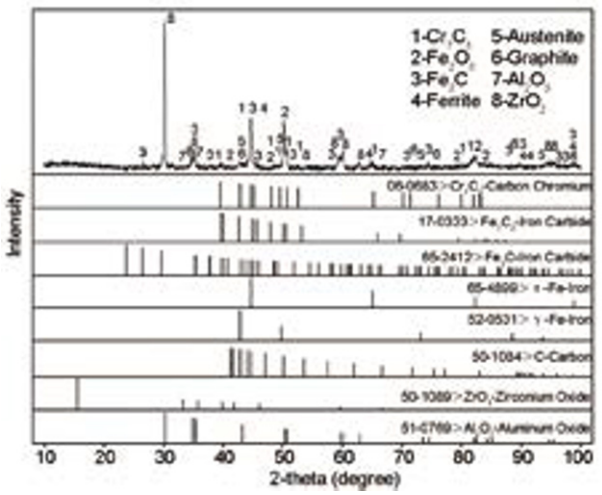

Fig. 3: X-ray diffraction pattern of ATZ ceramic particles reinforced gray iron matrix surface composite

2.3 Microstructural analysis

Figure 4 gives the SEM images of the metallurgical structure of the ATZ ceramic particle reinforced gray iron matrix surface composites. The graphite, lamellar pearlite, ledeburite, blocky and lath-shaped carbides are all observed in the solidified structure. Figure 5 exhibits the distribution of Fe and Cr elements and the chemical compositions of chromium alloyed products in the composite. It can be observed that Fe and Cr elements exist in all carbides [Fig. 5 (c) and (f)], and because of the close atomic radius of Fe and Cr atoms, interstitial solid solution and substitutional solid solution are formed in the composite. The results show that the atomic ratio of (Fe+Cr)/C are about 7:3 and 3:1, respectively [Fig. 5 (a) and (d)]. This conclusion can be obtained that the lath-shaped carbide is M_3C phase and the blocky carbide is M_7C_3. To further identify the blocky carbide as M_7C_3 and the lath-shaped carbide as M_3C phase, their microhardnesses are also measured under a load of 1 kgf and dwelling time of 15 s. The values are 855–1,100 HV and 1,620–1,850 HV, respectively, which agree with Kagawa's findings [23].

2.4 Wear behavior characterization

To understand the effects of ATZ ceramic particle reinforcement and chromium surface alloying on wear behavior and

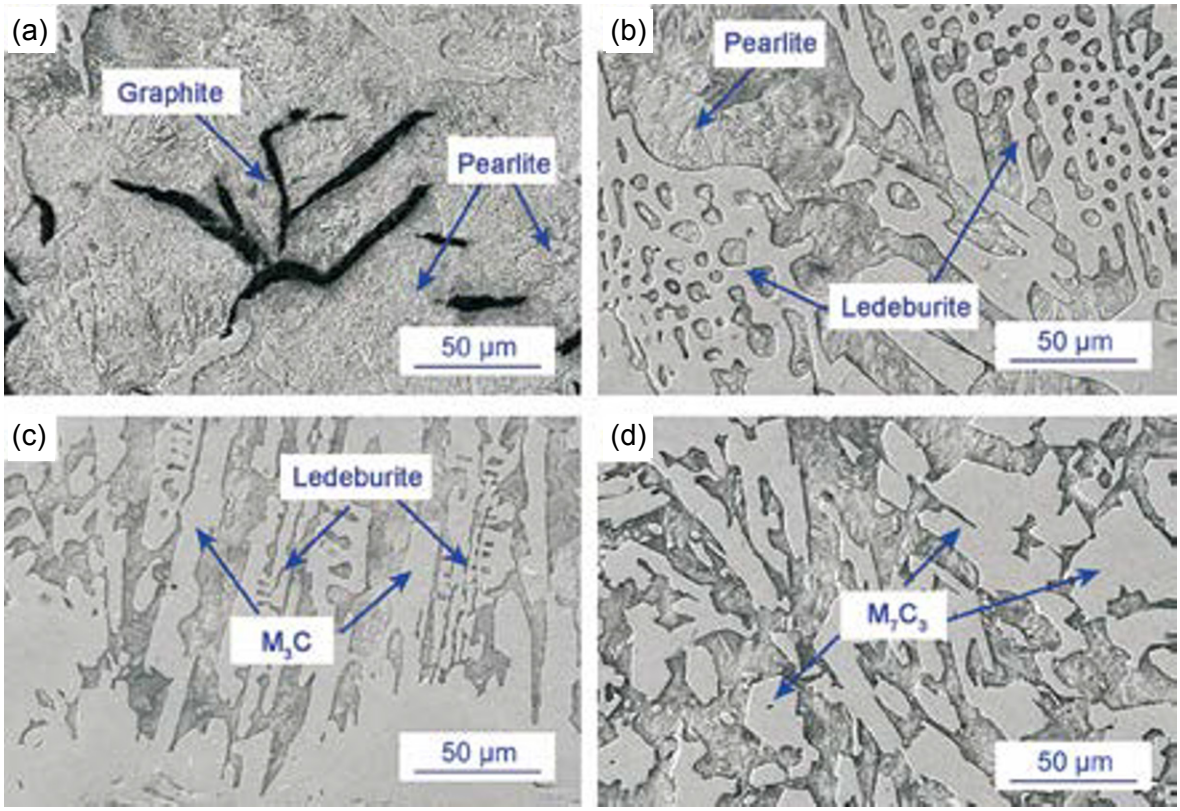

Fig. 4: SEM images of chromium alloyed products in composite

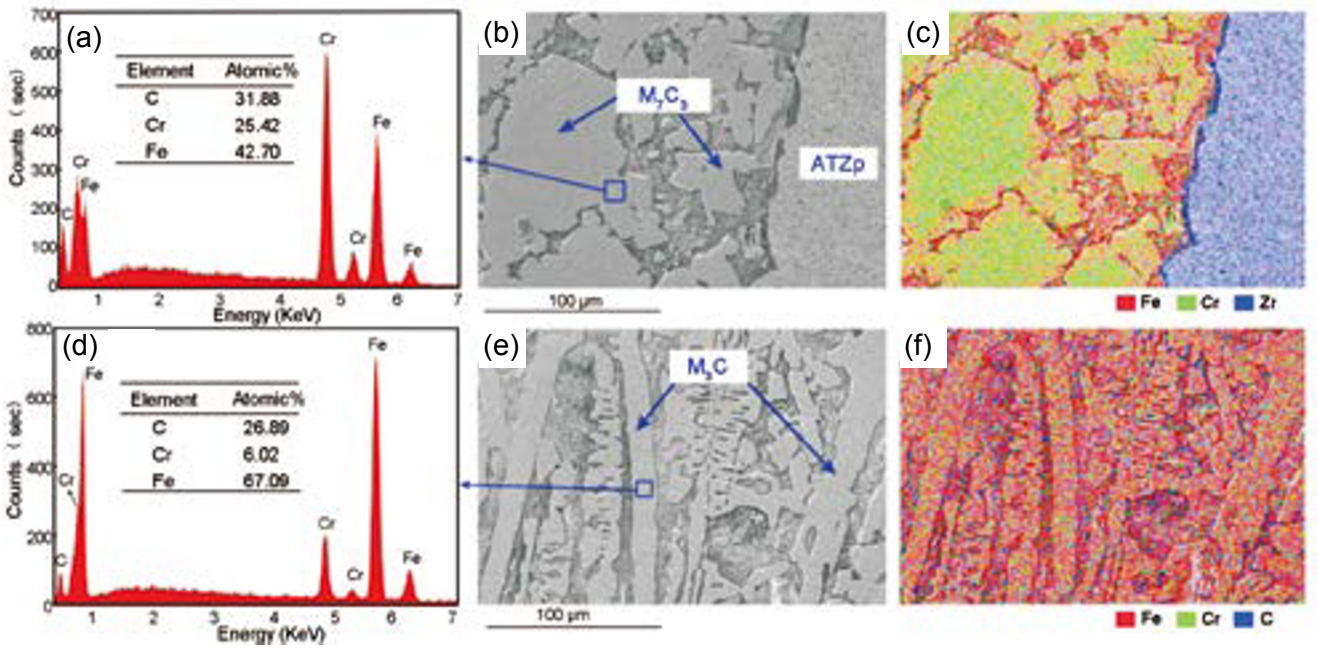

Fig. 5: Chemical compositions of alloyed products in composite

mechanism of the composite, the volumetric wear rate and worn surfaceof ATZ ceramic particle reinforced gray iron matrix surface composite (S1), chromium surface alloyed gray iron (S2), ATZ ceramic particles reinforced gray iron matrix composite (S3), and gray iron (S4) were measured and observed. Figure 6(a) shows the relationship between wear volume losses of the selected specimens and wheel revolution. It can be observed that the wear volume losses of S1 to S4 increase with the number of revolutions increasing. The changing trend of wear volume losses of S2 and S4 is linear, while the wear volume losses trend of S1 and S3 is nonlinear. The volumetric wear rates of S1 to S4 are plotted in Fig. 6(b). The volumetric wear rates of S2 and S4 remain unchanged, but those of S1 and S3 decrease to a steady-state after a certain period of wear testing. The wear resistance of S1 is 2.7 times higher than that of S4. The results show that both ATZ ceramic particle reinforcement and chromium surface alloying improve the wear resistance of gray iron matrix.

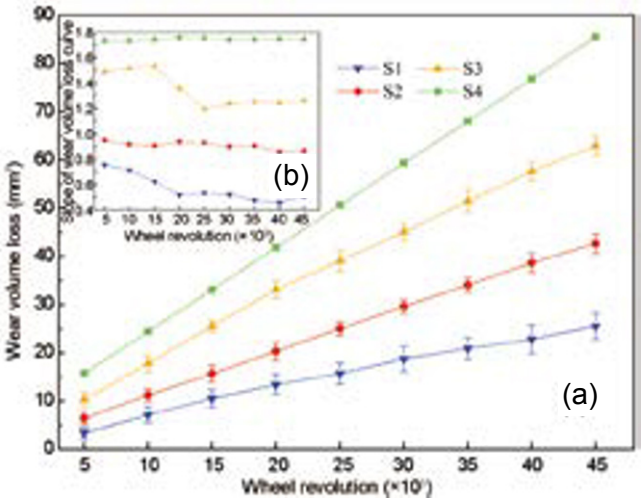

Fig. 6: Wear behavior of specimens with different wheel revolutions: (a) volumetric wear and (b) slope of volumetric wear curve

2.5 Wear mechanism of composite

Comparing S1 with S2, the volumetric wear rates of S1 and S2 show little difference at the initial stages of wear testing. When the number of revolutions increases to 20,000, the volumetric wear rate of S1 decreases to a steady-state. A similar phenomenon is also observed in the wear behaviors of S3 and S4 [cf. Fig. 6 (b)]. The reason is that ATZ ceramic particles and metal matrix are in the same plane at the initial stage of wear testing, the hardness of ATZ ceramic particles (1,250–1,280 HV) and quartz abrasive particles (800–1,200 HV) are higher than that of gray iron matrix (200–300 HV). With the wear time increasing, the gray iron is concave and the ATZ ceramic particles bulge due to the volumetric wear rate of gray iron matrix being greater than that of ATZ ceramic particle. The bulged ceramic particles can protect the gray iron matrix around them, and the gray iron matrix also support ceramic particles (cf. Fig. 7). This phenomenon can be called shadow effect. The shadow effect does not play a role at the initial stages of wear testing because ATZ ceramic particles and gray iron matrix are in the same plane. With the wear time increasing, the ATZ ceramic particles bulge and resist the main wear force of the abrasive, so the volumetric wear rates of S1 and S3 significantly reduce and then tend to be a steady-state.

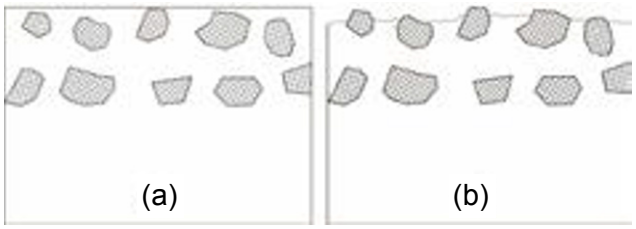

Fig. 7: Schematic illustration of wear mechanism of composite: (a) before wear and (b) after wear

To explore the effect of chromium surface alloying on wear behavior of ATZ ceramic particle reinforced gray iron matrix surface composite, the wear behaviors of S1 and S3 were investigated. The volumetric wear rate of S3 is higher than that of S1 [Fig. 6(b)]. This indicates that chromium surface alloyed can effectively improve the wear resistance of the composite. Figure 8 presents the SEM images of wear morphology of S1 and S3. As revealed in the figures, there are significant differences between the worn surfaces of S1 and S3. The wear morphology of S3 contains many furrows of abrasive wear. The furrows are probably produced by the cutting of abrasive particles, due to the hardness of the quartz abrasive particles, 800–1,200 HV, higher than that of gray iron matrix, 200–300 HV. The furrows are not observed at the wear morphology of S1, but many carbides protruding are exposed at the surface.

The difference of wear morphology between S1 and S3 is believed due to their distinct surface hardnesses. The abrasive wear rate can be simply calculated by the following formula based on the mechanism of micro-cutting [24]:

$$\frac{dV}{ds} = k_{\alpha} \frac{W}{H} \quad (1)$$

where, dV/ds is the wear capacity rate [$mm^3 \cdot (N \cdot m)^{-1}$], W is the carrying load of each abrasive particle (N), H is the hardness (HV) and k_{α} is the constant depending on the hardness, shape and number of abrasive particles in cutting.

The above equation indicates that increasing the hardness

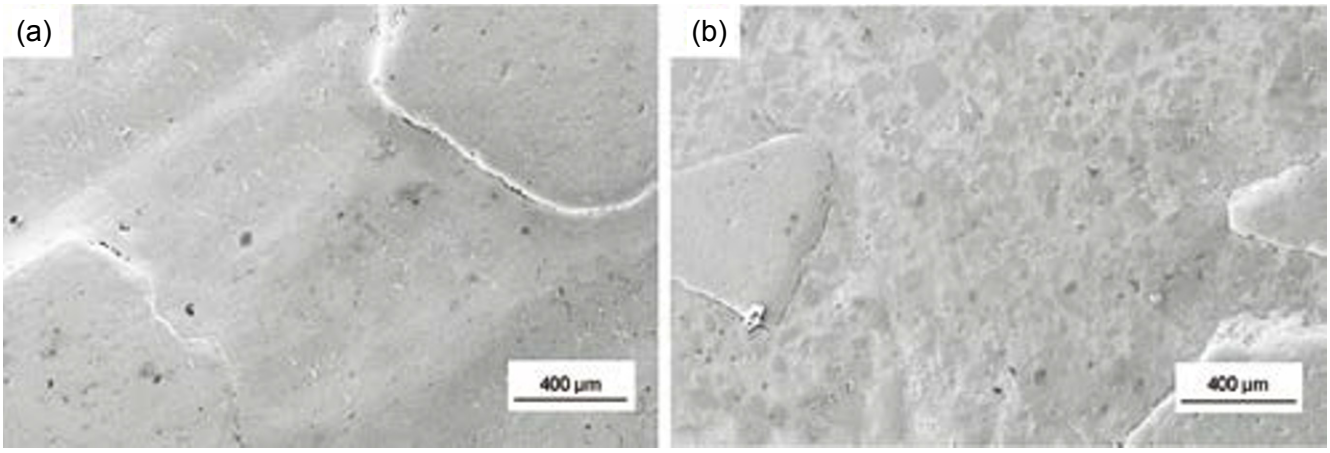

Fig. 8: SEM images of wear morphology of (a) S3 and (b) S1

value of the composite can be used to improve the abrasion resistance of abrasive grain. The addition of HCFPs increases the average surface hardness value of gray iron matrix from 200–300 HV to 500–600 HV. So the hardness difference between the abrasive particle and gray iron matrix decreases, and the cutting effects on substrate of abrasive particle reduces significantly. In addition, the raised rigid carbides also start to bear the wear force of abrasive particles after the surface layer of matrix wears off. As a result, the wear resistance of S1 improves remarkably due to both the surface hardness increase of gray iron matrix and ATZ ceramic particles protecting effect.

3 Conclusions

In the present work, a porous preform with HCFPs, borax, binder and ATZ ceramic particles was first produced and then an ATZ ceramic particle reinforced and chromium surface alloyed gray iron matrix composite was successfully produced by the pressureless infiltration. The following conclusions can be drawn:

(1) The addition of HCFPs leads to the formation of white iron during solidification. The phase constitutions of the composite consist of ATZ ceramic, α-Fe, γ-Fe, graphite, ledeburite, pearlite, M_3C, and M_7C_3.

(2) The wear volume loss rate of ATZ ceramic particle reinforced gray iron matrix surface composite decreases first, then tends to be stable. The wear resistance of the composite is approximately 2.7 times higher than that of gray iron matrix.

(3) The mechanism of wear resistance increase is a combination of the surface hardness increase of iron matrix and ATZ ceramic particles and alloy carbides protecting effect on gray iron matrix.

References

[1] Philip A, Schweitzer P E. Metallic Materials: Physical, Mechanical, and Corrosion Properties. New York: NY: Marcel Dekker Inc., 2003: 1–8.
[2] Tomlinson W J, Cash M, Bransden A S. Dry sliding wear of grey iron laser surface alloyed with 14-40% chromium. Wear, 1991, 142(2): 383–386.
[3] Tang S L, Gao Y M, Li Y F. Recent developments in fabrication of ceramic particle reinforced iron matrix wear resistant surface composite using infiltration casting technology. Ironmaking and Steelmaking, 2014, 48(1): 633–640.
[4] Jarzabek D M, Chmielewski M, Wojciechowski T. The measurement of the adhesion force between ceramic particles and metal matrix in ceramic reinforced-metal matrix composites. Composites Part A: Applied Science and Manufacturing, 2015, 76: 124–130.
[5] Krauss G, Kübler J and Trentini E. Preparation and properties of pressureless infiltrated SiC and AlN particulate reinforced metal ceramic composites based on bronze and iron alloys. Materials Science and Engineering: A, 2002, 337(1): 315–322.
[6] Rabiei A, Vendra L and Kishi T. Fracture behavior of particle reinforced metal matrix composites. Composites Part A: Applied Science and Manufacturing, 2008, 39(2): 294–300.
[7] Zhang Fan, Wang Lige and Wang Enze. A review of preparation techniques for ceramic particles reinforced iron matrix composites. Powder Metallurgy Industry, 2015, 25 (2) 63–69. (In Chinese)
[8] Anasori B, El'ad N C and Barsoum M W. Fabrication and mechanical properties of pressureless melt infiltrated magnesium alloy composites reinforced with TiC and Ti_2AlC particles. Materials Science and Engineering: A, 2014, 618: 511–522.
[9] Zhang Q, Ma X and Wu G. Interfacial microstructure of SiCp/Al composite produced by the pressureless infiltration technique. Ceramics International, 2013, 39(5): 4893–4897.
[10] Zhang P, Zeng S L, Zhang Z G, et al. Microstructure and hardness of WC-Co particle reinforced iron matrix surface composite. China Foundry, 2013, 10(6): 374–379.
[11] Boostani A F, Tahamtan S, Jiang Z Y, et al. Enhanced tensile properties of aluminium matrix composites reinforced with graphene encapsulated SiC nanoparticles. Composites Part A: Applied Science and Manufacturing, 2015, 68: 155–163.
[12] Kaftelen H, Unlu N, Goller G, et al. Comparative processing-structure–property studies of Al-Cu matrix composites reinforced with TiC particulates. Composites Part A: Applied Science and Manufacturing, 2011, 42(7): 812–824.
[13] Li Z, Jiang Y, Zhou R, Lu D H, et al. Dry three-body abrasive wear behavior of WC reinforced iron matrix surface composites produced by V-EPC infiltration casting process. Wear, 2007, 262(5): 649–654.
[14] Zheng K H, Gao Y M, Li Y F, et al. Three-body abrasive wear resistance of iron matrix composites reinforced with ceramic particles. Proceedings of the Institution of Mechanical Engineers, Part J: Journal of Engineering Tribology, 2014, 228(1): 3–10.
[15] Vadiraj A, Balachandran G, Kamaraj M, et al. Studies on mechanical and wear properties of alloyed hypereutectic gray cast irons in the as-cast pearlitic and austempered conditions. Materials & Design, 2010, 31(2): 951–955.
[16] Wang Y, Pan Z Y, Wang Z, et al. Sliding wear behavior of Cr-Mo-Cu alloy cast irons with and without nano-additives. Wear, 2011, 271(11): 2953–2962.
[17] Wiengmoon A, Pearce J T H and Chairuangsri T. Relationship between microstructure, hardness and corrosion resistance in 20wt.% Cr, 27wt.% Cr and 36wt.% Cr high chromium cast irons. Materials Chemistry and Physics, 2011, 125(3): 739–748.
[18] Amirsadeghi A. and Sohi M H. Comparison of the influence of molybdenum and chromium TIG surface alloying on the microstructure, hardness and wear resistance of ADI. Journal of Materials Processing Technology, 2008, 201(1): 673–677.
[19] Durand J M, Vardavoulias M and Jeandin M. Role of reinforcing ceramic particles in the wear behaviour of polymer-based model composites. Wear, 1995, 181: 833–839.
[20] Kim T H and Kim B C. Chromium carbide laser-beam surface-alloying treatment on stainless steel. Journal of Materials Science, 1992, 27(11): 2967–2973.
[21] Durand-Charre M. Microstructure of Steels and Cast Irons. New York: NY: Springer, 2004: 124.
[22] Xiao B, Xing J D, Feng J, et al. A comparative study of Cr_7C_3, Fe_3C and Fe_2B in cast iron both from ab initio calculations and experiments. Journal of Physics D: Applied Physics, 2009, 42(11): 115415.
[23] Kagawa A, Okamoto T, Saito K et al. Hot hardness of $(Fe, Cr)_3C$ and $(Fe, Cr)_7C_3$ carbides. Journal of Materials Science, 1984, 19(8): 2546–2554.
[24] Wen S Z and Huang P. Principles of Tribology. Singapore: John Wiley & Sons, 2012: 369.

This work was financially supported by the Scientific Research Fund of SiChuan Provincial Education Department (No. 17ZA0395) and the Doctoral Program Foundation of Southwest University of Science and Technology (No. 10zx7113).